

The Structure of Narrow-Line Region in LINERs *

Hai-Feng Dai and Ting-Gui Wang

Center for Astrophysics, University of Science and Technology of China, Hefei 230026, China;
twang@ustc.edu.cn, daihfh@mail.ustc.edu.cn
Joint Institute of Galaxies and Cosmology, Shanghai Observatory and USTC, China

Received 2007 September 3; accepted 2007 October 13

Abstract Low-ionization nuclear emission regions (LINERs) are present in a large fraction of local galaxies, while their connection to the more luminous active galactic nuclei (AGN) remains elusive. We analyze the narrow band images obtained by the Hubble Space Telescope (*HST*) in $H\alpha$ + $[NII]$ and/or $[OIII]$ band for 23 LINERs and low luminosity Seyfert galaxies in the sample of the Palomar Optical Spectroscopic Survey of nearby galaxies in an attempt to resolve the structure of Narrow Emission Line Regions (NLRs) of these objects. In all cases, NLRs are well resolved and their morphology differs from object to object. Clumps, linear structure, spiral arms or a ring are detected in a large fraction of the objects, while there is no significant difference between Seyfert galaxies and LINERs. We find that the NLR size and the narrow line luminosity are strongly correlated for both LINERs and low luminosity Seyfert galaxies, and that the size of $H\alpha$ + $[NII]$ emission line region scales with $H\alpha$ luminosity as $R_{NLR} \propto L_{H\alpha}^{0.44 \pm 0.06}$, consistent with an extension of the NLR size-luminosity relation defined for luminous Seyfert galaxies and quasars, to two orders of magnitude lower in luminosity and to lower activity levels. Our results suggest that NLRs in LINERs are similar to those of Seyfert galaxies, and they are powered by the central active galactic nucleus.

Key words: galaxies: active — galaxies: Seyfert — galaxies: structure — LINER

1 INTRODUCTION

The emission line spectra of active galactic nuclei show both broad and narrow structures. The narrow lines have widths typically of $200 < \text{FWHM} < 500 \text{ km s}^{-1}$, often with high velocity tails for the high ionization lines. The Narrow emission Line Region (NLR) is of great interest because it is the only AGN component that is spatially resolved optically, and because its width traces the potential of the host galactic bulge (Peterson 1997). With a scale from a few tens of parsecs in low luminosity active galactic nucleus (LLAGN) up to several kpc in quasars, the NLR is the largest structure that dominates the source of energy input in active galactic nuclei (AGNs) apart from the giant radio structures in radio galaxies and quasars. It can be directly imaged with the current ground and space telescopes for nearby AGNs. Previous $[OIII]$ images obtained by *HST* have revealed elongated “ionization cone” structures that coincide with the extended radio structures (e.g., Capetti et al. 1996; Falcke et al. 1998; Schmitt et al. 2003; Bennert et al. 2006). The ionization cone is considered as evidence for the presence of an axisymmetric dust torus in the AGN on parsec scales which constitutes an important ingredient in the unification scheme of broad and narrow lined AGN (Antonucci 1993). Spatially resolved spectroscopy from *HST* provides rich information on the physics and kinematics of the emission line gas in the NLR. A detailed comparison of line ratios of individual clumps with photoionization models has suggested that the NLR is mainly ionized by the central AGN, while shocks and young stars are of much less importance (Whittle et al. 2005).

* Supported by the National Natural Science Foundation of China.

However, some fundamental questions still remain. What physical process determines the size of the NLR? What drives the complex kinematics of gas in the NLR? A key step towards the answers is to establish an empirical relation between the size of the NLR and various observables. Bennert et al. (2002) noticed, for a sample of seven PG quasars and seven Seyfert galaxies, that the NLR size scales with [OIII] luminosities as $R_{[\text{OIII}]} \propto L_{[\text{OIII}]}^{0.5}$. Schmitt et al. (2003) found a substantially flatter slope (0.33 ± 0.04) for a sample of 60 Seyfert galaxies, and (0.42 ± 0.03) after including the PG quasars. The latter authors found also larger scatters. However, it is not clear whether this change in the slope is real or is merely due to uncertainties in the measurements/contamination. Therefore, extension of the observations to a large dynamic range to lower luminosity is required.

Low level nuclear activities are common among local bright galaxies. In the Palomar Optical Spectroscopic Survey of a sample of 486 nearby galaxies, Ho, Filippenko & Sargent (1995, 1997a,b) found that about 33% of the galaxies can be classified as Low-Ionization Nuclear Emission Region (LINER). However, it is still not clear at present what their physical nature is and what fraction they are of genuine AGNs. Plausible models include photoionization by a non-stellar continuum source, such as LLAGN, collisional ionization by fast shocks (Heckman 1980), and photoionization by UV radiation generated by clusters of hot, young stars (e.g., Terlevich & Melnick 1985; Shields 1992). Clearly, high spatial resolution image of NLRs can provide important clues to this problem. If LINERs are similar objects with scaled-down nuclear activity, they might show a similar morphology to the NLRs, and follow the same size-luminosity relation. The *HST* observations revealed that some LINERs indeed show ionization cone(s) and linear structures that are often seen in Seyfert galaxies (Pogge et al. 2000).

In this paper, by analyzing a sample of LINERs and low luminosity Seyfert galaxies we investigate: (1) Whether the NLR size-luminosity relation for Seyfert galaxies and quasars can be extended to much lower luminosities; (2) Whether LINERs have similar NLR morphology as Seyfert galaxies; and (3) Whether LINERs follow the same NLR size-luminosity relation. The paper is organized as follows. The sample and data reduction will be described in Section 2. NLR morphology and size for the sample of low luminosity AGNs are presented in Section 3. We discuss the implication of results in the last section. Through out this paper we adopt cosmology constants of $H_0 = 75 \text{ km s}^{-1} \text{ Mpc}^{-1}$, $\omega_\lambda = 0.72$ and $\omega_m = 0.27$.

2 THE SAMPLE AND DATA REDUCTIONS

Ho et al. (1995, 1997a,b) carried out a spectroscopic survey of a complete magnitude limit sample of 486 nearby bright galaxies, and classified the emission line galaxies in their samples into AGN and HII galaxies. We extracted LINERs and low luminosity ($L_{\text{H}\alpha} \leq 10^{40} \text{ erg s}^{-1}$) Seyfert galaxies from the sample of Ho et al. (1995, 1997a,b) and cross-correlated with the *HST* data, to search for objects that have narrow band [OIII] or/and $\text{H}\alpha + [\text{NII}]$ images. A total of 25 objects, including six low luminosity Seyfert galaxies and 19 LINERs, have been observed with WFPC2 in [OIII] or/and $\text{H}\alpha + [\text{NII}]$ (with filters F656N or F658N) bands.

We retrieved the broad and narrow band WFPC2 images of these objects from the *HST* archive, which had been processed by standard OPUS pipeline with the most recent calibration files. The images have been flat-fielded, dark corrected, hot-pixel masked and thus require only minimal postprocessing to give images in physical units. All the galaxies are located on PC1 chips with a pixel scale of $0.04554'' \text{ pixel}^{-1}$ except NGC 3031 and NGC 4438, which are on the Wide Field Camera ($0.1'' \text{ pixel}^{-1}$). Table 1 summarizes the observations, including the filters, total exposure times, and the observing program ID. All galaxies except NGC 4258 were observed through either the F656N or the F658N filters. Five of the galaxies have narrow [OIII]-band images. Most observations were split into several exposures to allow for cosmic ray rejection. To subtract the underlying continuum, images of adjacent continua were taken in broad-band filters (F547M, F555W, F569W, F675W, F702W and F791W) (Table 1).

All the subsequent data processing was done using the IRAF tasks. Images with multiple exposures of the same band were combined, and cosmic ray hits were removed using the IRAF task CRREJ during the process. When only one exposure was available, cosmic ray hits were removed manually using the task CRMEDIAN. We did not try to subtract sky background at the first stage for either on- or off-band images because this would be done at the subsequent subtraction.

The Continuum-subtracted emission-line images were created by subtraction of the associated continuum. First we register (spatially align) the narrow-band (or on-band) and broad-band (off-band) images using field stars to determine the relative shift and rotation of the two images (cf. Pogge 1992). Centroids

Table 1 Objects and Exposure Time

Object	F502N	F656N	F658N	F547M	F555W	F569W	F675W	F702W	F791W	Program(GO/GTO)
NGC 2787	2800	800	...	6785
NGC 3718	4200	720	6436
NGC 3998	1600	240	5924
NGC 4036	2800	300	5419,6785
NGC 4192	5000	2600	...	720	5419,6436
NGC 4278	12700	600	6731
NGC 4438	...	5200	5200	1450	6791
NGC 4636	2500	500	8031,8686
NGC 5005	2400	...	1400	720	6436,5419
NGC 404	...	1700	...	350	5999,6871
NGC 2768	2800	800	6785
NGC 3623	1800	1800	8591
NGC 4111	1200	600	6785
NGC 4314	600	600	6265
NGC 4374	2600	1200	6094
NGC 4486	2700	800	5122
NGC 4594	1600	1340	5122,5924
NGC 4736	...	1700	296	8591,5741
NGC 3031	...	1800	...	90	5986
NGC 4258	2300	...	2300	1116	5123
NGC 4579	3200	...	1400	726	6436
NGC 4472	3400	...	460	6673
NGC 5194	1700	1800	...	860	5123

NOTES: Exposure time (in second) is given in the appropriate column for each objects and filters. Last column gives the *HST* program numbers under which the observations were carried out.

are measured for stars common to both images and the mean shift and rotating angle of the off-band image relative to the on-band image are computed. In most cases, we cannot find three or more stars common to the two images. Galactic centers are searched though the task STARFIND or IMCNT. Once the shift and rotation have been determined, the off-band image is shifted and re-binned to match the on-band image. We adopt an interpolation scheme using spline function during the rebinning in order to conserve the total flux. Because the data in the on-band image are of interest, we re-bin the off-band images.

To the first order, the scaling factor between the continuum of off-band and on-band filters is just the bandwidth of their bandpasses multiplied by their exposure time. If the continuum shape is flat between the two bandpasses to the first order, the relative number of continuum photons passed by each filter is determined by their relative width, peak transmissions and exposure times. Scaling and subtraction of continuum image are carried out iteratively. By modifying the guess value according to the statistics in the continuum-subtracted image, we make the median in the emission-line free region to converge eventually be close to zero.

Finally, we removed two objects from the initial sample of 25 AGNs. We excluded NGC 3079, because there were large dust lanes covering the emission line region just above and below the nucleus which would affect the size measurement of the NLRs. We also excluded NGC 1052 because no usable continuum band image of it was available. This leaves a sample of 23 objects (22 have $H\alpha$ + $[NII]$ images, six have $[OIII]$ images, while NGC 4278 has only an $[OIII]$ image).

3 RESULTS

The NLRs are resolved for all the objects in the sample (Figs. 1, 2 and 3). In the following, we will describe some individual objects endowed with relatively complex structures. NGC 4036 shows a bright tail to the south-west direction, a fainter and more diffuse tail in the opposite direction, and a dark region just above the center in $H\alpha$ + $[NII]$ image. This type of morphology may be caused by a small scale dust lane or even by a torus. If this is the case, then the south-west is the near side. NGC 5194 has a similar structure near its central region. The $[OIII]$ emission of NGC 4278 comes mostly from a bright nuclear component, surrounded by a symmetric ring. Both the $[OIII]$ and $H\alpha$ + $[NII]$ images of NGC 4258 show a bright nuclear

Table 2 Basic Properties and Results

Object	Hubble Type	Distance (Mpc)	Scale (pc arcsec ⁻¹)	B_T (mag)	Class	$\log L_{H\alpha}^a$ (erg s ⁻¹)	$R_{H\alpha}$ (pc)	$\log L_{[OIII]}$ (erg s ⁻¹)	$R_{[OIII]}$ (pc)
NGC 2787	SB(r)0	13.0	63.0257	11.82	L1.9	38.52	103.33
NGC 3718	SB(s)a	17.0	82.4182	11.59	L1.9	38.46L	85.58
NGC 3998	SA(r)0	21.6	104.7196	11.61	L1.9	40.00	154.51
NGC 4036	SA0	24.6	119.2640	11.57	L1.9	39.35	136.87
NGC 4192	SAB(s)a	16.8	81.4486	10.95	L1.9	38.97	133.53	38.12b	7.79
NGC 4278	E1	9.7	47.0269	11.09	L1.9	38.88	48.83
NGC 4438	SA(s)0/a	16.8	81.4486	11.02	L1.9	39.37	165.80
NGC 4636	E0	17.0	82.4182	10.43	L1.9	38.27	29.28
NGC 5005	SAB(rs)bc	21.3	103.2652	10.61	L1.9	39.47	220.09	39.41	126.97
NGC 404	SA(s)0	2.4	11.6355	11.21	L2.0	37.63	8.58
NGC 2768	E6	23.7	114.9007	10.84	L2.0	39.01L	149.13
NGC 3623	SAB(rs)a	7.3	35.3913	10.25	L2.0	37.77	52.70
NGC 4111	SA(r)0	17.0	82.4182	11.63	L2.0	39.40	212.81
NGC 4314	SB(rs)a	9.70	47.0268	11.43	L2.0	38.45	20.56
NGC 4374	E1	16.8	81.4486	10.09	L2.0	38.89	154.67
NGC 4486	E0	16.8	81.4486	9.59	L2.0	39.44	170.25
NGC 4594	SA(s)a	20.0	96.9626	8.98	L2.0	39.70	211.95
NGC 4736	(R)SA(r)ab	4.3	20.8470	8.99	L2.0	37.75	41.58
NGC 3031	SA(s)ab	1.4	6.7874	7.89	S1.5	37.64L	25.80
NGC 4258	SAB(s)bc	6.8	32.9673	9.10	S1.9	38.35	30.63	38.77	28.83
NGC 4579	SAB(rs)b	16.8	81.4486	10.48	S1.9	39.44	133.53	39.42b	56.52
NGC 4472	E2	16.8	81.4486	9.37	S2.0	37.59	38.95
NGC 5194	SA(s)bc	7.7	37.3306	8.96	S2.0	38.88L	51.00	38.91	49.47

NOTES: ^a ‘L’ denotes a lower limit. Values with uncertainties of $\pm 30\%$ – 50% are followed by “b” (see Ho et al. 1997a,b)

component and a one-side spiral structure. The off-nuclear extended bright knots in $H\alpha$ + $[NII]$ are certainly due to star-forming activity because the correspondent features in $[OIII]$ are much weaker. The spiral arms are also present in the $H\alpha$ + $[NII]$ image of NGC 4736. Bright knots in a ring of size $6''$ are also seen on the $H\alpha$ + $[NII]$ images of NGC 4314, and can be ascribed to the star-formation activity (Knapen et al. 2006). $H\alpha$ + $[NII]$ filaments surround the nucleus of NGC 4374 and NGC 4486, while filaments are seen on one side of the nucleus in NGC 404. NGC 4438 displays a hat-like $H\alpha$ + $[NII]$ image, the upper and low parts are obscured by dust lanes which are seen both in the broad and narrow band images. In NGC 4111 and NGC 4594, the $H\alpha$ emission is aligned with the large scale galaxy disk. NGC 5194 shows a bright nuclear component, an off-nucleus clump and weak knots over the whole galaxy in $H\alpha$ + $[NII]$. The $[OIII]$ emission is relative weak for the off-nucleus clump, suggesting that it is powered by star-formation activity. NGC 4486 (M87), a giant elliptical galaxy, has an obvious one-side optical jet with some-knots in the raw images. The jet disappears in the emission line map, suggesting that no emission line region is associated with the radio jet, while its $H\alpha$ + $[NII]$ emission comes from a relative small, asymmetrical region. Pogge et al. (2000) have presented in detail some of these objects covered by their sample.

Following Benert et al. (2002), we define the size of the NLR as the radius of an annulus at which a 3σ -level above background is reached. Note with this definition, extended diffuse emission usually does not affect our measurement. In fact, obvious star-forming regions mentioned above are all beyond the NLR size given in this paper. A conservative estimate suggests that these radii can be off by ~ 2 pixels ($0.091''$ for PC1, and $0.2''$ for WF3) according to their surface brightness profiles (see also Schmitt et al. 2003). It is quoted as the uncertainty of the NLR size in Table 2.

The angular radius ranges from 1 to a few arcsec for those objects. The physical sizes at their redshifts are in range of less than 10 parsec to 250 parsec, which are obviously smaller than normal NLRs of Seyfert galaxies and PG quasars. We found that the size of the $H\alpha$ emission regions is always larger than the size of the $[OIII]$ emission regions by a factor of typically 3–4, for both LINERs and low-luminosity Seyfert galaxies that have both $[OIII]$ and $H\alpha$ + $[NII]$ images available.

One of our purposes is to check whether a similar NLR size-luminosity correlation is present also for LINERs. In Figure 4, we plot the NLR size versus the narrow $H\alpha$ luminosity for LINERs and low

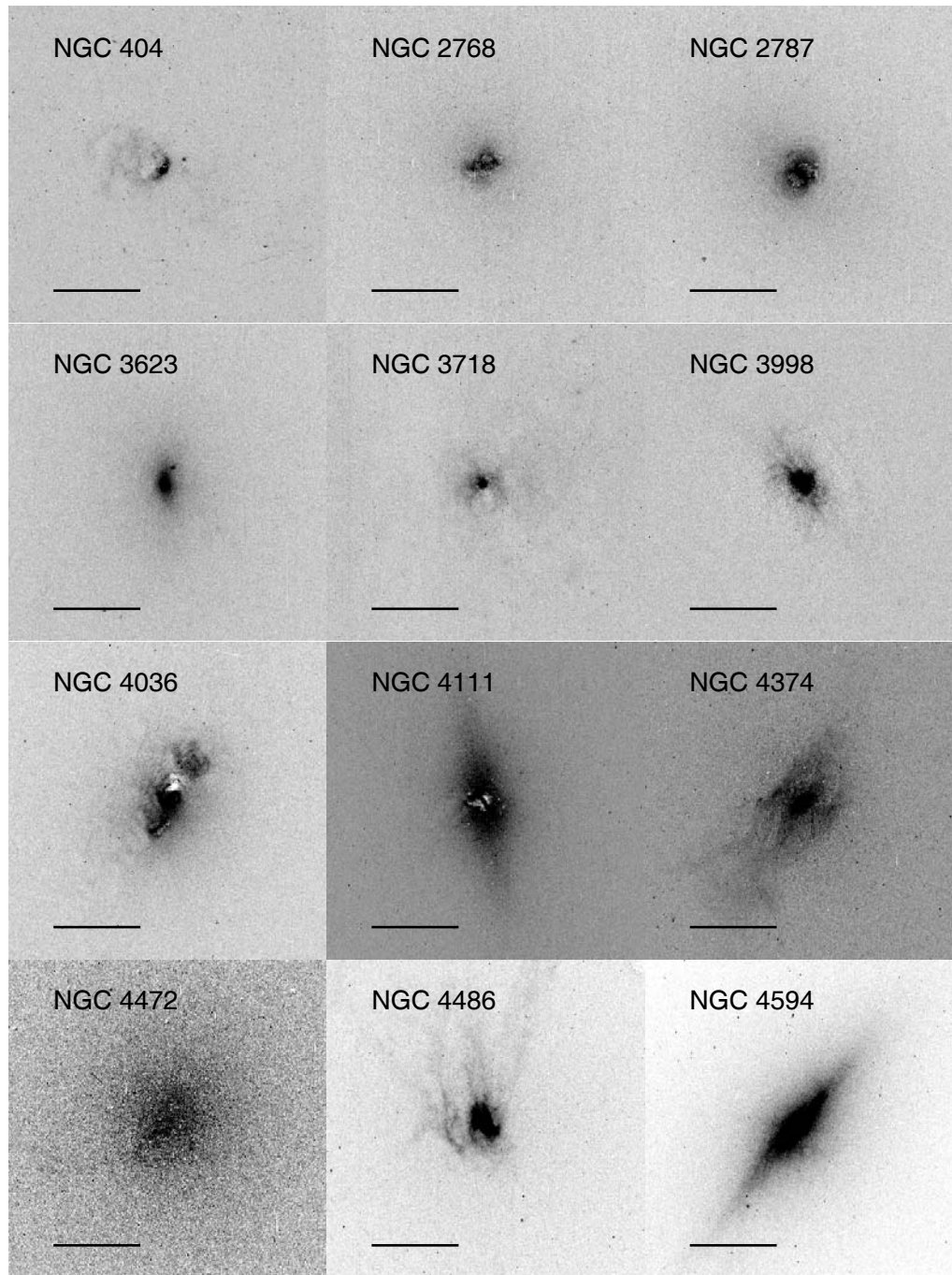


Fig. 1 Continuum-subtracted H α + [NII] images. Each panel shows a 400 pixel \times 400 pixel segment of the image centered on the nucleus and the horizontal bar in the lower left corner marks off 5".

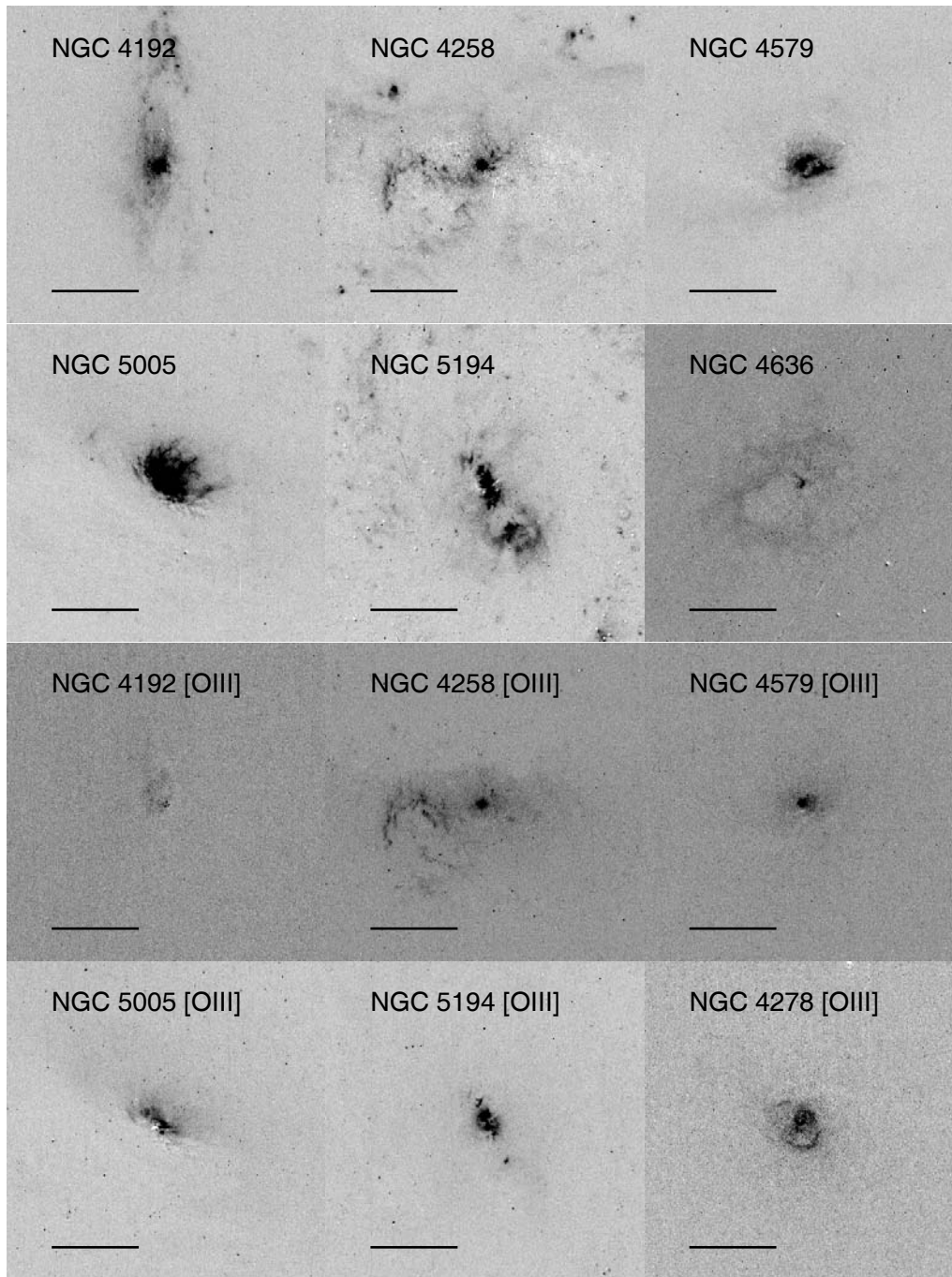


Fig. 2 Continuum-subtracted images. The upper six images are $H\alpha + [NII]$ emission, the rest are $[OIII]$ emission images. The marked scale bar is 5".

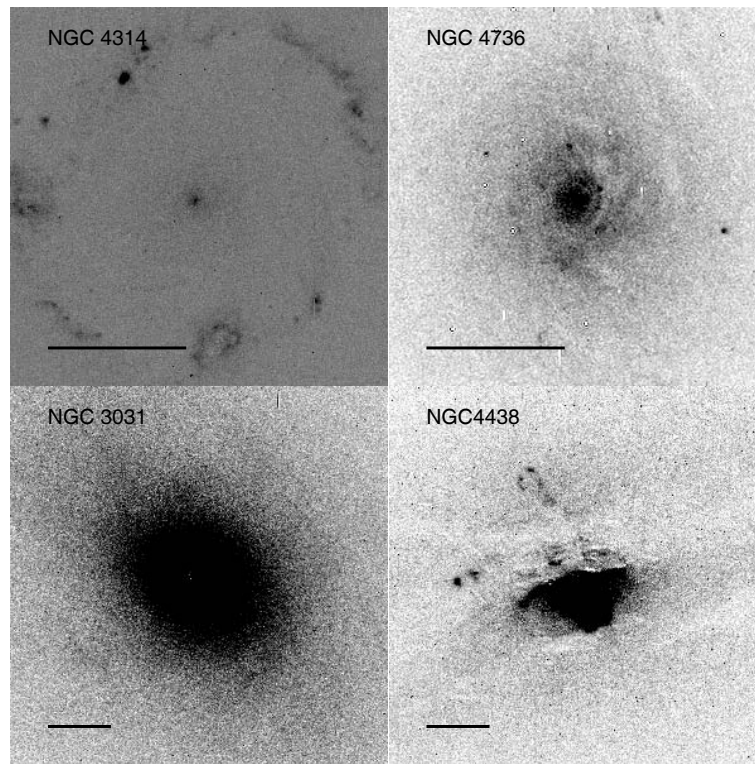


Fig. 3 Two images observed with the nucleus positioned on the PC CCD. In the case of NGC 3031 and NGC 4438, the nuclei were positioned on the WF3 CCD. We show the panel with 300 pixels \times 300 pixels centered on the nucleus and the scale bar in the lower left corner of each image is about 5''.

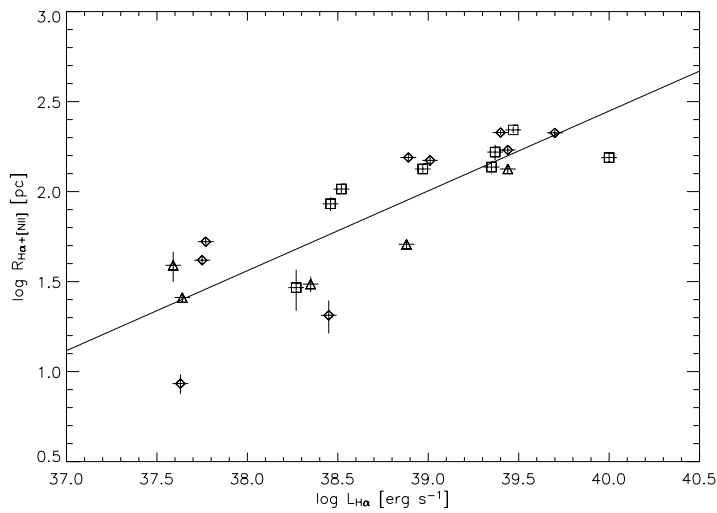


Fig. 4 NLR size versus the narrow $H\alpha$ luminosity for low luminosity AGNs. The open diamonds represent LINER 2s, squares represent LINER 1.9s, and triangles represent low luminosity Seyfert galaxies. The solid line show best weighted fit $R \propto L_{H\alpha}^{0.44 \pm 0.06}$. The error bars indicate the uncertainties in the apertures about two pixels. The error for $L_{H\alpha}$ is about 10% (Ho et al. 1997a).

luminosity Seyfert galaxies. The narrow $H\alpha$ luminosities were taken from Ho et al. (1997), while only sizes of $H\alpha+[NII]$ are plotted. The NLR size and narrow $H\alpha$ line luminosity are evidently correlated. It should be noted that five dwarf Seyfert galaxies follow almost the same correlation. Therefore, we fit these galaxies and the LINERs together. With a Spearman rank correlation coefficient of $r_s = 0.87$ for 22 objects, the probability for the null hypothesis is very small (1.5×10^{-07}). A weighted linear fit in the log-log yields a slope of 0.39 ± 0.01 when the uncertainty of the NLR size is considered. However, the reduced $\chi^2(36)$ is very large, so an unweighted fit is preferred, which gives:

$$\log(R_{\text{NLR,pc}}) = (0.44 \pm 0.06) \log(L_{H\alpha}) - (13.29 \pm 0.30). \quad (1)$$

To check whether dwarf Seyfert galaxies and LINERs are on an extension of the same correlation found for luminous Seyfert galaxies and quasars, we plot the size of [OIII] emission line region versus [OIII] luminosity for six objects (three low-luminosity Seyfert galaxies and three LINERs) in the sample, and for the Seyfert galaxies and quasars from Bennert et al. (2002) and Schmitt et al. (2003). See Figure 5. We can find in the figure that LINERs and low luminosity Seyfert galaxies are on a simple extension of the NLR size-luminosity correlation to lower luminosities, without any apparent break in the slope. For all those objects, a log-log fit to the [OIII] size versus [OIII] luminosity yields:¹

$$\log(R_{\text{NLR,pc}}) = (0.47 \pm 0.03) \log(L_{[\text{OIII}]}) - (16.63 \pm 1.04). \quad (2)$$

Though the sample of low luminosity AGN with [OIII] image is still very small, we noticed that if the sizes of the $H\alpha$ emission region are divided by a factor of 3, the average size ratio of $H\alpha$ to [OIII] for the five objects with both [OIII] and $H\alpha$ images available, and the LINERs and low luminosity Seyfert galaxies are located also on the extension of the correlation (Fig. 5).

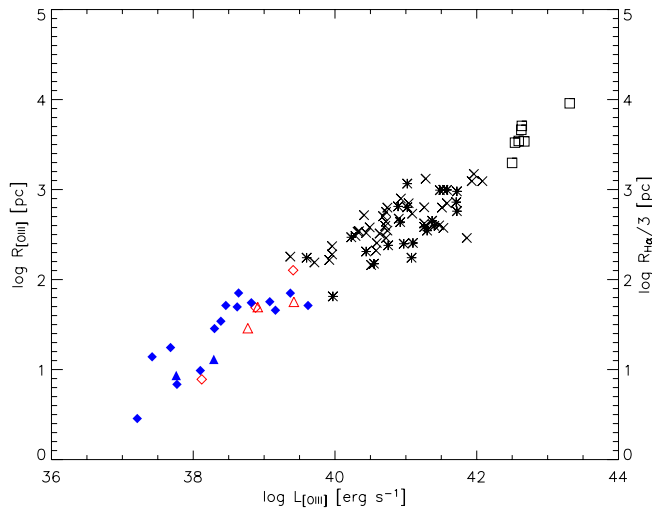


Fig. 5 [OIII] luminosity versus NLR size of PG quasars, Seyferts and low luminosity AGNs. The legends are: squares for PG quasars (Bennert et al. 2002), asterisks for Seyfert 1 galaxies, crosses for Seyfert 2 galaxies (Schmitt et al. 2003), the open diamonds represent $R_{[\text{OIII}]}$ of LINERs, the open triangles represent $R_{[\text{OIII}]}$ of low-luminosity Seyfert galaxies. The filled diamonds and triangles represent $R_{H\alpha}/3$ of LINERs and low luminosity Seyferts without [OIII] images, respectively.

¹ Both luminosity and size in Bennert et al. (2002) and Schmitt et al. (2003) have been converted to values for a value of $H_0 = 75 \text{ km s}^{-1} \text{ Mpc}^{-1}$.

4 CONCLUSIONS AND DISCUSSION

Low luminosity AGNs show a variety of emission line morphologies in $H\alpha+[NII]$, including spiral structure, a ring, knots and filaments that usually surround a bright nuclear component. For five objects with available [OIII] and $H\alpha+[NII]$ images, we found that the [OIII] emission region is more compact and shows less frequently of complex structure. Some of the complex structures in $H\alpha+[NII]$ may be ascribed to circum-nuclear star-forming activity, while some others may be due to obscuration by a dust torus that bends the ionizing continuum into a conical structure, or due to the obscuration of a galactic dust lane in front of the NLR, or due to the interaction of a radio emitting plasma with interstellar medium. We did not find systematic differences between type 1 and type 2 LINERs, or between Seyfert galaxies and LINERs, although the sample for the dwarf Seyfert galaxies is still very small.

We found that the size of $H\alpha$ emission region is well correlated with the $H\alpha$ luminosity for low luminosity Seyfert galaxies and LINERs. This correlation is a natural extension of a similar correlation between the size of [OIII] emission region and [OIII] luminosity for luminous Seyfert galaxies and quasars. Combining our low luminosity AGN sample with luminous Seyfert and quasars, we showed that the NLR size scales with the narrow line luminosity as $R_{NLR} \propto L^{0.5}$ for more than 3 orders in size or 6 orders in luminosity, as well as for very different activity levels.

The similarity in the structure of NLRs of LINERs and low luminosity Seyfert galaxies to those of the more luminous Seyfert galaxies and quasars suggests that a common physical process, probably photoionization by AGN continuum, predominates in these objects as well. This view is consistent with the correlations between the optical emission lines and the ionizing continuum (Ho & Peng 2001) or the X-ray emission (Terashima et al. 2000; Ho et al. 2001).

Evidence for a large fraction of LINERs being genuine AGN has been mounting in recent years. Although only 25% of LINERs harbor a compact emission of UV, from an analysis of galaxy disk inclinations, Maoz et al. (1995) and Barth et al. (1998) found that the fraction of UV-bright LINERs may be close to 50%. Unresolved hard X-ray core is found in 75% of the high-resolution Chandra HRI images (Ho et al. 2001), including all type I LINERs and the majority of type II LINERs. Radio imaging surveys have shown some strong evidence for nonstellar processes in LINERs (e.g., Nagar et al. 2000; Falcke et al. 2000; Filho, Barthel & Ho 2000, 2002a,b): 64% of the LINER 1s, 36% of the LINER 2s and 25% of the transition objects have a compact radio core. VLA and VLBI showed that about 60%–80% LINERs have compact radio core, and high brightness temperature ($\geq 10^7$ K). Our results add one more note to the origin of LINERs: they not only harbor low luminosity AGNs, their emission line regions are also essentially similar to those of Seyfert galaxies.

Acknowledgements The authors thank W. Zhang, H.Y. Zhou, X. B. Dong for their kind helps for the data reduction. This work was funded by the NSFC through Grant 10573015.

References

- Antonucci R. R. J., 1993, ARA&A, 31, 473
- Barth A. J., Ho L. C., Filippenko A. V., 2000, AAS, 177, 2108
- Barth A. J., Ho L. C., Filippenko A. V., 1998, ApJ, 496, 133
- Bennert N., Falcke H., Schulz H. et al., 2002, ApJ, 574L, 105
- Bennert N., Junfwiert B., Komossa S. et al., 2006 A&A, 456, 953
- Bennert N., Junfwiert B., Komossa S. et al., 2006 A&A, 459, 55
- Capetti A., Axon D. J., Macchetto F. et al., 1996, ApJ, 469, 554
- Eracleous M., Shields J. C., Chartas G. et al., 2001, ApJ, 565, 108
- Falcke H., Nagar N. M., Wilson A. S. et al., 2000, ApJ, 542, 197
- Falcke H., Wilson A. S., Simpson C., 1998, ApJ, 502, 199
- Filho M. E., Barthel P. D., Ho L. C., 2001, ASPC, 249, 703
- Filho M. E., Barthel P. D., Ho L. C., 2002, ApJS, 142, 223 (2002a)
- Filho M. E., Barthel P. D., Ho L. C., 2002, A&A, 385, 425 (2002b)
- Filippenko A. V., Ho L. C., 2003, ApJ, 588, 13
- Heckman T. M., 1980, A&A, 87, 152
- Ho L. C., Peng C. Y., 2001, ApJ, 555, 650

- Ho L. C., 2001, ASPC, 284, 13
- Ho L. C., Filippenko A. V., Sargent W. L. W., 1995, ApJS, 98, 477 (Paper II)
- Ho L. C., Filippenko A. V., Sargent W. L. W., 1997, ApJS, 112, 315 (1997a)
- Ho L. C., Filippenko A. V., Sargent W. L. W. et al., 1997, ApJS, 112, 391 (1997b)
- Ho L. C., Filippenko A. V., Sargent W. L. W., 2003, ApJ, 583, 159
- Maoz D., Filippenko A. V., Ho L. C. et al., 1995, ApJ, 404, 91
- Nagar N. M., Wilson A. S., Falcke H., 2001, ApJ, 559, L87
- Peterson B. M., 1997, An introduction to active galactic nuclei, 1st ed., London: Cambridge
- Pogge R. W., 1992, ASPC, 23, 195
- Pogge R. W., Maoz D., Ho L. C. et al., 2000, ApJ, 532, 323
- Schmitt H. R., Donley J. L., Antonucci R. R. J. et al., 2003, ApJS, 148, 327
- Shields J. C., 1992, ApJS, 399L,27
- Terashima Y., Ho L. C., Ptak A. F., 2000, ApJ, 539, 161
- Terlevich R., Melnick J., 1985, MNRAS, 213, 841
- Whittle M., Rosario D. J., Silverman J. D. et al., 2005, AJ, 129, 104